

## 32. NEOGENE PALEOCEANOGRAPHY AND PALEOCLIMATE HISTORY FROM FRAM STRAIT: CHANGES IN ACCUMULATION RATES<sup>1</sup>

Suzanne O'Connell,<sup>2</sup> Thomas C.W. Wolf-Welling,<sup>3</sup> Michel Cremer,<sup>4</sup> and Rüdiger Stein<sup>5</sup>

### ABSTRACT

Changes in coarse fraction, calcium carbonate, and total organic carbon (TOC) accumulation rates and wt% define four different Neogene climatic and oceanographic regimes for the deep-water Fram Strait area (Site 909). These changes are not as well developed in intermediate water depth at Site 908, possibly indicative of differences in current velocities at the two sites. Stage I, upper lower to middle Miocene (Site 909, 838–1062 meters below seafloor [mbsf]; 17.5–10.85 m.y.), sediments consist of a fining-upwards sequence of mass-wasted sediments, interbedded with laminated and bioturbated sediments. Tectonic influences are the dominant control on these sediments, which were deposited before the initiation of sustained bottom-water flow through Fram Strait.

Stage II, from middle to upper Miocene (Site 909, 838–368 mbsf; 10.85–5.7 m.y.; Site 908, 185–167 mbsf; 6.2–5.7 m.y.), shows the greatest variation in bulk and coarse fraction accumulation rates. It consists of two step-wise increases in bulk accumulation rate, followed by a rapid decrease. In each sequence, after the increase begins, the number of layers with high nonbiogenic carbonate increases, and an increase in the amount and variability of the coarse fraction follows. When the accumulation rate decreases, the coarse component decreases first, followed by a decrease in nonbiogenic carbonate and then the total accumulation rate decrease follows. The changes are most likely a result of the initiation and/or major increase of glaciation and the build-up of ice sheets, accompanied by changes in bottom-water strength. The first dropstones were recovered during Stage III, upper Miocene to middle Pliocene (Site 909, 368–200 mbsf; Site 908, 167–104 mbsf; 5.7 to 2.8 m.y.), during which the coarse fraction accumulation rates are low (<1000 gcm<sup>-2</sup>m.y.<sup>-1</sup>). In fact there is surprisingly little variation in coarse fraction accumulation. However, higher accumulation rates and a slight increase in coarse components is observed at Site 908 4.2–2.8 Ma. Stage IV, middle Pliocene to the present (<2.8 m.y.), from 200 to 0 mbsf at Site 909 and from 105 to 0 mbsf at Site 908, contains high-amplitude variations in coarse fraction and %TOC attributable to glacial-interglacial fluctuations. With the exception of very low rates between 1.1 and 2.0 m.y. at Site 908, coarse fraction accumulation rates are higher at Site 908 than at Site 909, and they may indicate changes in bottom-water strength and/or different source areas.

### INTRODUCTION

Fram Strait, located between Greenland and Spitsbergen at a depth of 2600 m, is the primary deep-water connection between the Arctic and Atlantic Oceans (Swift et al., 1983; Kristoffersen, 1990). During Ocean Drilling Program (ODP) Leg 151 a two-site depth transect was cored in Fram Strait, Sites 908 and 909 (Fig. 1).

Site 908 (78°23.112'N, 1°21.637'E) was drilled on the Hovgård Ridge in 1277 m of water. Hovgård Ridge marks the northern boundary of the Boreas Basin and the southern boundary of the deep Fram Strait. This site was cored to determine the age and lithologies of sediments in basins on the ridge crest, to explore the history of water mass exchange between the Arctic Ocean and the Norwegian-Greenland Sea, and to establish the timing and sedimentary processes after the opening of Fram Strait. Two holes were drilled at this site with the advanced hydraulic piston corer/extended core barrel (APC/XCB). Hole 908A penetrated 345 m, reaching Oligocene age sediment and Hole 908B penetrated 83 m of Pleistocene sediment.

Site 909 (78°35.096'N, 3°4.222'E) was drilled on a small abyssal terrace directly north of the Hovgård Ridge and approximately in the center of Fram Strait. Located at 2518 meters below sea level (mbsl), this site was cored to investigate the timing of the opening of a deep-water connection between the Arctic and Atlantic Oceans and to provide a record of the onset and evolution of Arctic glacial history and climate variability. Three holes were drilled at this site: Hole 909A was cored with the advanced hydraulic piston corer/extended core barrel (APC/XCB) to a depth of 92.5 meters below seafloor (mbsf); Hole 909B was also cored with the APC/XCB to a depth of 135.1 mbsf; and Hole 909C was cored with the rotary corer to a depth of 1061.6 mbsf.

### LITHOLOGY

The Neogene sections of Sites 908 and 909 are dominated by siliclastic sediments; the sections are generally much thicker at Site 909. The Miocene section is almost totally missing from Site 908 (Fig. 2), where thin upper Miocene sediments unconformably overlie Oligocene silty clay with 8%–20% biosilica. The unconformity is marked by two silty to sandy glauconite layers, interpreted to have formed from altered ash (Myhre, Thiede, Firth, et al., 1995). In contrast, the Miocene section at Site 909 is 700 m thick.

The Pleistocene through upper Miocene section at Site 908 (0–185 mbsf) consists of one lithologic unit, separated into three sub-units on the basis of sedimentary structures. The upward trend is toward more variable size range, including large dropstones (Fig. 2). Subunit IA (0–81.4 mbsf), which is Pleistocene to Pliocene in age, contains widely varying grain sizes and dropstones are common.

<sup>1</sup>Thiede, J., Myhre, A.M., Firth, J.V., Johnson, G.L., and Ruddiman, W.F. (Eds.), 1996. *Proc. ODP, Sci. Results*, 151: College Station, TX (Ocean Drilling Program).

<sup>2</sup>Department of Earth and Environmental Sciences, Wesleyan University, Middletown, CT 06459, U.S.A. soconnell@wesleyan.edu

<sup>3</sup>GEOMAR, Wischhofstraße 1-3, Building 4, D-24148 Kiel, Federal Republic of Germany.

<sup>4</sup>Département de Géologie et Océanographie, Université de Bordeaux I, Avenue des Facultés, 33405 Talence cedex, France 3.

<sup>5</sup>Alfred Wegner Institute, Columbusstraße 2, D-27568 Bremerhaven, Federal Republic of Germany.

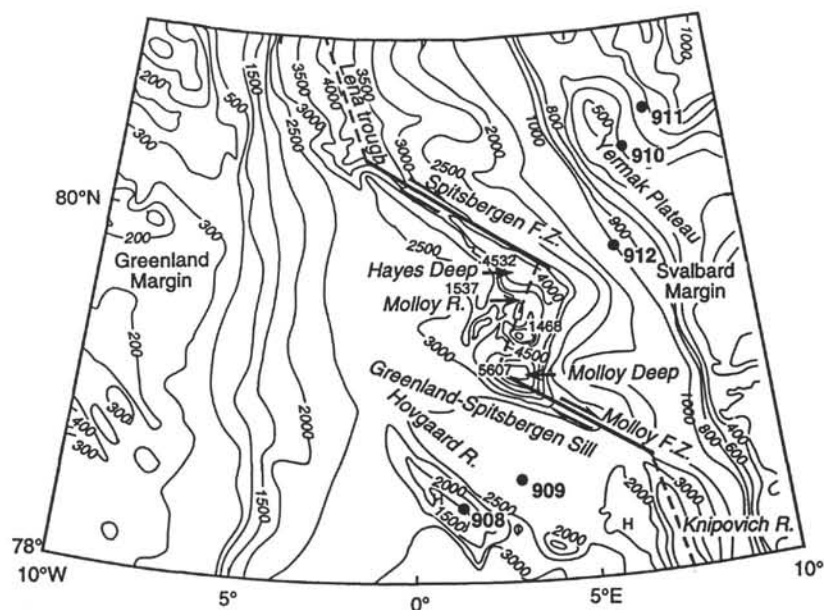


Figure 1. Location of Sites 908 and 909 in Fram Strait and Sites 910, 911, and 912 on the Yermak Plateau.

Sediments are defined as clayey mud, silty mud, and silty clay. Subunit IB (81.4–139.2 mbsf) consists of silty clay, and clayey silt, and fewer dropstones. Subunit IC (139.2–185 mbsf), Pliocene to late Miocene in age, consists of silty clay with no dropstones.

The thicker section at Site 909 has been divided into to three units. The upper two units, Pleistocene to late Miocene in age, are similar to the equivalent age section at Site 908. Unit I (0–248.8 m) contains common to abundant dropstones and consists of interbedded clay, silty clay, and clayey mud, with a minor component of calcareous nannofossils in the upper 50 m (Fig. 3). Unit II (248.8–518.3) contains fewer dropstones and is dominated by very dark gray silty clay and clayey silt with common pyrite (Fig. 4). Unit III, late and middle Miocene in age, is separated into two subunits. Subunit IIIA (518.3–923.5 mbsf) contains meter-scale intervals of bioturbated and laminated layers, and Subunit IIIB (923.5–1061.8 mbsf) contains contorted and folded beds and redeposited clasts (Fig. 5).

## METHODS

Percentages and accumulation rates of  $\text{CaCO}_3$ , total organic carbon (TOC) and coarse fraction are reported here, by depth and age. Calcium carbonate values were generated by two different methods. A Coulometrics acidification module was used shipboard and at Wesleyan University. For these measurements, samples were freeze-dried and approximately 0.5 g were extracted, hand ground to powder, and weighed. A subsample of approximately 0.1 g was acidified in the heated reaction vessel with hydrochloric acid to form carbon dioxide, which was transferred into an absorption cell. The absorption cell contained an aqueous medium of ethanolamine and a coulometric indicator. The interaction of  $\text{CO}_2$  and the cell forms a base electrically and titrates to an end point determined by optical transmission of the indicator (Huffman, 1977). The pulse output was scaled and fed to a counter that registers  $\mu\text{g C}$ . When all of the  $\text{CO}_2$  had been evolved and titrated, as recognized by a stable Coulometer reading, the registers  $\mu\text{g C}$  reading was taken and the results were calculated as  $\% \text{CaCO}_3$  ( $\% \text{CaCO}_3 = \% \text{C}_{\text{inorg}} \times 8.334$ ). A laboratory standard and a blank were run after every eight samples. Blank values were subtracted from the reading  $\mu\text{g C}$ . Repeat measurements were reproducible with an accuracy of 1%. Values that were significantly different (5%) than values above and below were rerun twice more and the average of the two values was used.

Additional carbonate measurements were made in conjunction with TOC measurements at GEOMAR, where TOC was measured using a Leco CS-125. Total carbon (TC) was measured first. After treatment with hydrochloric acid and removal of the inorganic carbon (IC), the total organic carbon (TOC) was measured. The inorganic carbon was assumed to be bound as  $\text{CaCO}_3$  and was calculated as  $(\text{IC} = \text{TC} - \text{TOC}) \times 8.33$ .

Shipboard measurements of TOC were made using a Carlo Erba Model NA 1500 CNS analyzer. Total organic carbon was calculated from the difference between total carbon (TC) and inorganic carbon.

Sand percentages were determined by wet sieving. Approximately 10 g of dried sample was weighed and placed in an Erlenmeyer flask with 100–150 ml of deionized water. Samples were soaked and placed in an automatic shaker at 180 rpm for approximately 24 hr. After the sample was disaggregated, it was washed from the flask into a 63- $\mu\text{m}$  sieve. Material from the sieve was washed into a tin dish and oven dried at 40–60°C. The dried sample was weighed and stored.

Accumulation rates were calculated from shipboard measurements of dry bulk density and linear sedimentation rates based on shipboard paleomagnetic age determinations and revised biostratigraphic picks available at the post-cruise meeting (Tables 1, 2). Because microfossils were generally scarce and age datums not always well defined, paleomagnetic age determinations were generally used. However, paleomagnetic age determinations suffer from incomplete core recovery and core disturbance. Therefore, age data is often a limiting factor.

## RESULTS

Information is presented in both tables (Tables 3, 4 on CD-ROM in back pocket of this volume) and graphs, and the graphs show information plotted vs. depth (Figs. 7, 9) and age (Figs. 8, 10).

### Bulk Accumulation and Sedimentation Rates

Bulk accumulation rates were generally high at both sites, with Site 909 rates being consistently higher. The lowest values were found at the base of each section and include the entire middle Miocene at Site 909 and the lower Pliocene and uppermost Miocene section at Site 908. In addition, there are several intervals of about 0.5 m.y. or shorter at Site 909 where bulk accumulation rates are close to

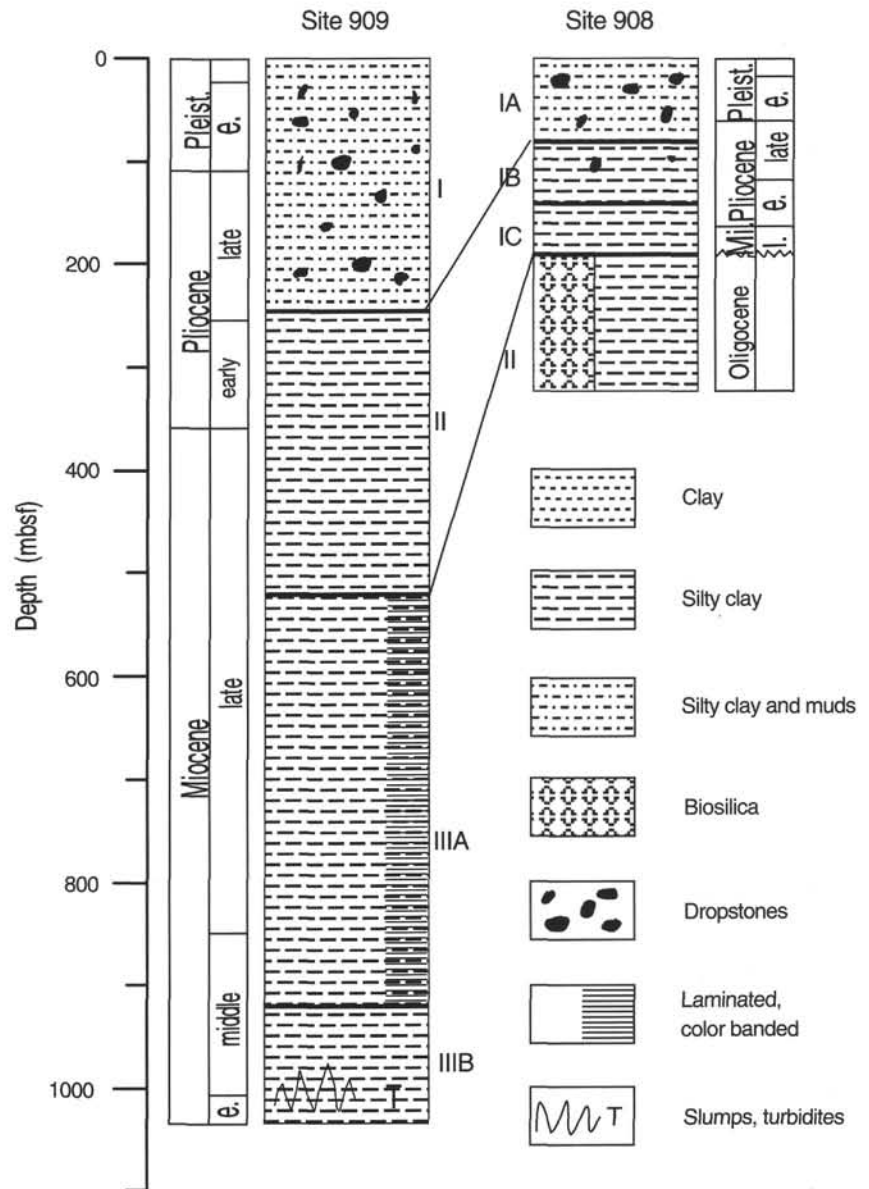


Figure 2. Lithologic summary of Sites 908 and 909.

or less than  $5000 \text{ gcm}^{-2}\text{m.y.}^{-1}$  (e.g., 8–8.5, 5–5.5, and 4.3–4.4 m.y.). The lowest accumulation rates are found at Site 908, where a 0.9-m.y. interval from 1.1 to 2.0 m.y. has accumulation rates between 570 and  $800 \text{ gcm}^{-2}\text{m.y.}^{-1}$ . The highest accumulation rates ( $21,000\text{--}25,000 \text{ gcm}^{-2}\text{m.y.}^{-1}$ ) occur at Site 909 and were sustained for more than 1 m.y. from 5.7 to 7.25 m.y. Accumulation rates were most variable between 4 and 6 m.y. at Site 909.

Linear sedimentation rates were also very high (Fig. 6) and ranged from a low of 4.4 m/m.y. (1.1–2.0 m.y.) to 118.46 m/m.y. (0.99–1.06 m.y.) at Site 908. At Site 909, sedimentation rates ranged from 25.7 m/m.y. (5.06–5.72 m.y.) to 174.6 m/m.y. (4.71–4.82 m.y.).

### Calcium Carbonate Content

Carbonate content is extremely low at both sites, averaging around 1% by weight. Average carbonate accumulation rates are less than  $400 \text{ gcm}^{-2}\text{m.y.}^{-1}$  at Site 909 and less than  $100 \text{ gcm}^{-2}\text{m.y.}^{-1}$  at Site 908. Isolated, thin, high-carbonate layers contain up to 60% carbonate by weight or  $10,000 \text{ gcm}^{-2}\text{m.y.}^{-1}$  at Site 909. The carbonate in

these peaks is nonbiogenic and is both detrital and authigenic (see Chow et al., this volume), although each layer was not examined in detail and some layers may also contain detrital carbonate. The middle Miocene section (Site 909) contains the fewest number carbonate-rich layers as well as the ones with the lowest percentage of carbonate. The upper Miocene section (Site 909) shows the most variation in accumulation rates, which can be grouped into four intervals of high and low variation in carbonate-rich layers accumulation with durations of 1.7–1.2 m.y. These intervals transcend changes in sedimentation rates and are readily identifiable on the depth sections, so they are not just a function of changing accumulation rates. The high-variation intervals, between 10.5 and 8.8 m.y. and 7.6 and 6.2 m.y., are slightly longer than the low-variation intervals.

The uppermost interval at Site 909 with a low number of carbonate-rich layers, 6.2–4.9 m.y., marks the beginning of a section that was recovered at both sites. Accumulation rates are an order of magnitude less at Site 908 than Site 909, and the number of carbonate-rich layers differs between the sites. At Site 908, variability is lowest between 5.2 and 2.7 m.y., with only one layer having an accumula-



Figure 3. Ice-rafted detritus and lithologic (silty mud to silty clay) and color (dark gray to very dark gray) variations (lithologic Unit I, Sample 151-909A-4H-2, 21–53 cm, 31.21–32.03 mbsf).



Figure 4. Fine-grained, very dark gray silty clay with pyrite concretions and poorly developed fissility (lithologic Unit II, Sample 151-909C-44R-1, 133–147 cm, 500.33–500.47 mbsf).



Figure 5. Very dark grayish brown clayey mud with laminated common coal and laminated silty clay clasts (lithologic Subunit IIIB, Sample 151-909C-90R-1, 141–124 cm, 943.94–944.04 mbsf).

tion rate  $>100 \text{ gcm}^{-2}\text{m.y.}^{-1}$ . In contrast, this interval has a high carbonate-rich layer variability at Site 909. At both sites there is high carbonate-rich layer variation and abundant data between roughly 2 and 2.6 to 2.7 m.y. Above this, there is an approximately 0.9-m.y. gap at Site 908 caused by low accumulation rates. The gap is represented at Site 909 by consistent accumulation rates between 2.0 and 1.4 m.y. and more variable rates between 1.4 and 1.1 m.y. In the upper 1 m.y., Site 909 has the lowest number of post-Miocene carbonate-rich layers. In contrast, at Site 908, variations are similar to those between 2.0 and 2.6 m.y., and slightly lower between 0.6 and 0.1 m.y. than between 1.0 and 0.6 m.y.

### TOC Accumulation

At Site 909, TOC values vary from 0.2% to 2.6% and average 0.9%. Values are lowest in the Pleistocene, which also has the highest amplitude variations, ranging from 0.2% to 1.4%. In the Pliocene and

upper Miocene values are higher, ranging from 0.8% to 1.7%. Most of the upper middle and middle middle Miocene is characterized by smaller amplitude variations and lower TOC%, roughly 0.8% to 1.2%. Beginning with a low value at about 950 mbsf and, with the exception of a second low value at approximately 1020 mbsf, the lower middle Miocene section is characterized by increasing TOC values, reaching a high of 2.6%. Accumulation rates vary from 10 to 500  $\text{gcm}^{-2}\text{m.y.}^{-1}$  and parallel the bulk accumulation rate, with the highest accumulation rates at around 4.7 m.y. and between 5.6 and 7.3 m.y.

TOC percentages at Site 908 are generally lower than at Site 909, and like Site 909, show high-amplitude variations (0.2% to 2.8%) in the Pleistocene, but, unlike Site 909, show a gradual increase in the Pleistocene through upper Miocene section.

### Coarse Fraction Accumulation

Sand percentages vary between 0% and 60% throughout most of both sites, but are generally less than 20% or  $2000 \text{ gcm}^{-2}\text{m.y.}^{-1}$ . The highest sand percentages occur in the lower middle Miocene, where a few samples contain as much as 80% sand, and upwards the percentage of coarse fraction decreases in repeated sequences 10 to 50 m thick and of 100,000 to 600,000 yr duration. Although the overall trend is fining upward cycles, there is a break at about 13.8 m.y. above a 25-m-thick, coarsening-upward interval (955–930 mbsf). In the middle to upper Miocene (9.9–6.8 m.y.) the sand fraction, like the carbonate fraction, contains alternating intervals of high and low sand. The high sand areas roughly correspond with the high carbonate spike areas, with the increase in carbonate spikes leading the increase in sand fraction and decreasing after the sand size decreases.

Between 6.8 and 2.8 m.y., sand accumulation at both sites is consistently low, with the exception of single high values near 6.3 m.y. Between 2.8 and 2.4 m.y. there are large variations in sand accumulation at Site 909. At Site 908 there is an increase in sand accumulation after 2.6 m.y., so that, in the interval between 2.6 and 2.0 m.y., sand accumulation rates are higher at Site 908. Between 1.5 and the present (1.0 at Site 908), sand accumulation shows wide variations, but with decreasing amplitude.

## DISCUSSION AND CONCLUSIONS

From the late early Miocene to the present, the Fram Strait region has been devoid of almost any biogenic sedimentation. This suggests low biological productivity or highly corrosive waters, as indicated by the lack of calcareous and siliceous microfossils in both shallow/intermediate- and deep-water sites. The biotic environment is in contrast to the Oligocene at Site 908, where biosilica, indicative of high productivity, composed about 8%–20% of the sediment. This suggests a major environmental change between the Oligocene unconformity (Site 908) and the early Miocene (Site 909).

The accumulation rates of the coarse fraction, carbonate, and organic carbon allow us to define four stages in the tectonic and climatic development of the Fram Strait region from the middle Miocene to the present (Table 5). Stage I ranges in age from late early to middle Miocene (Site 909, 1062–838 mbsf; 17.5–10.85 m.y.). Although it is within the range of North Atlantic sedimentation rates of 200–4000  $\text{cm/m.y.}$  (Davies et al., 1977), this interval contains the lowest sustained sedimentation rates (3340  $\text{cm/m.y.}$ ) and accumulation rates (7400–6000  $\text{gcm}^{-2}\text{m.y.}^{-1}$ ) at Site 909. The homogeneity of the sedimentation rates may, in part, be a result of the lack of age control. The upper interval of this stage is placed at a sedimentation rate change and below the boundary of a high-carbonate layer interval.

The high but decreasing sand percentages during Stage I, especially between the base of the section to about 14 m.y., are an excellent example of a fining-upwards sedimentary sequence. Slump structures are common at the base, and laminated intervals are inter-

bedded with nonlaminated beds. Carbonate content is also low, and high-carbonate layers are rare. TOC averages about 0.8% and has low-amplitude fluctuations, but it increases at the base. Because this interval is absent at Site 908, it is likely that sediments deposited on the surrounding plateaus and slopes were transported through mass wasting to the deeper Fram Strait basin. Therefore, the dominant control at the base of the section is attributed to sediment instability probably generated through tectonic events, most likely associated with crustal movement in Fram Strait. Upwards, interbedded laminated and bioturbated intervals indicate possible intermittent flow and ponding throughout this region. As the tectonic influence decreased, the importance of climatic and oceanographic factors increased. Size variations do not show any upward or downward trend above 14 m.y., and they may indicate changes in flow strength or possibly the initiation of ice rafting caused by minor glaciation.

Stage II ranges in age from middle to upper Miocene (Site 909: 838–368 mbsf, 10.85–5.7 m.y., Site 908: 185–167 mbsf, 6.2–5.7 m.y.). At Site 909, Stage II consists of two step-wise increases in bulk

accumulation rates, followed by abrupt drops. These changes are used to separate this stage into three substages. Stage II also includes the greatest variation in bulk sediment and carbonate accumulation rates, which vary between 5990 and 25800 gcm<sup>-2</sup>m.y.<sup>-1</sup> and 0 and 11315 gcm<sup>-2</sup>m.y.<sup>-1</sup>, respectively. The coarse fraction accumulation rates vary between 44 and 4700 gcm<sup>-2</sup>m.y.<sup>-1</sup> or 1% and 41%, in the 0.8–1.4 m.y. intervals previously described, and are bracketed by intervals of high-carbonate accumulation rate spikes. All three lines of evidence suggest major paleoclimatic and paleoceanographic changes. These include changes in both the volume of sediment and the provenance. Changes in provenance are suggested by variations in

**Table 2. Biostratigraphic and paleomagnetic age determinations for Site 909.**

Magnetic			Biostratigraphic		
Age (Ma)	Depth (mbsf)	Sedimentation rate (m/m.y.)	Age (Ma)	Depth (mbsf)	Sedimentation rate (m/m.y.)
0.00	0.00		0.00	0.00	
0.78	36.6	46.92			
0.98	44.3	37.75			
1.05	47.10	43.08	1.76	119.00	67.73
2.60	181.75	86.81			
3.55	247.00	68.47	3.55	393.00	152.56
4.26	295.00	67.42			
4.43	301.15	36.83			
4.61	313.75	70.39			
4.69	318.25	54.22			
4.81	338.85	174.58			
5.05	351.05	52.14	5.38	610.00	113.47
5.70	368.00	25.72			
7.25	590.00	144.16			
7.89	633.00	66.46			
8.53	657.00	37.68			
8.86	695.00	114.46			
9.59	762.40	92.20			
10.83	838.50	61.27	10.94	711.00	18.15
16.15	1016.15	33.42	16.15	1049.00	64.88

**Table 1. Paleomagnetic age determinations for Site 908.**

Age (Ma)	Depth (mbsf)	Sedimentation rate (m/m.y.)
0.00	0.00	
0.78	34.45	44.17
0.984	48.15	67.16
1.049	55.85	118.46
1.757	59	4.45
1.983	60	4.42
2.6	95.3	57.21
3.054	113	38.99
3.127	113.5	6.85
3.221	117	37.23
3.325	118	9.62
3.553	121.75	16.45
4.033	130	17.19
5.4	164.2	25.02

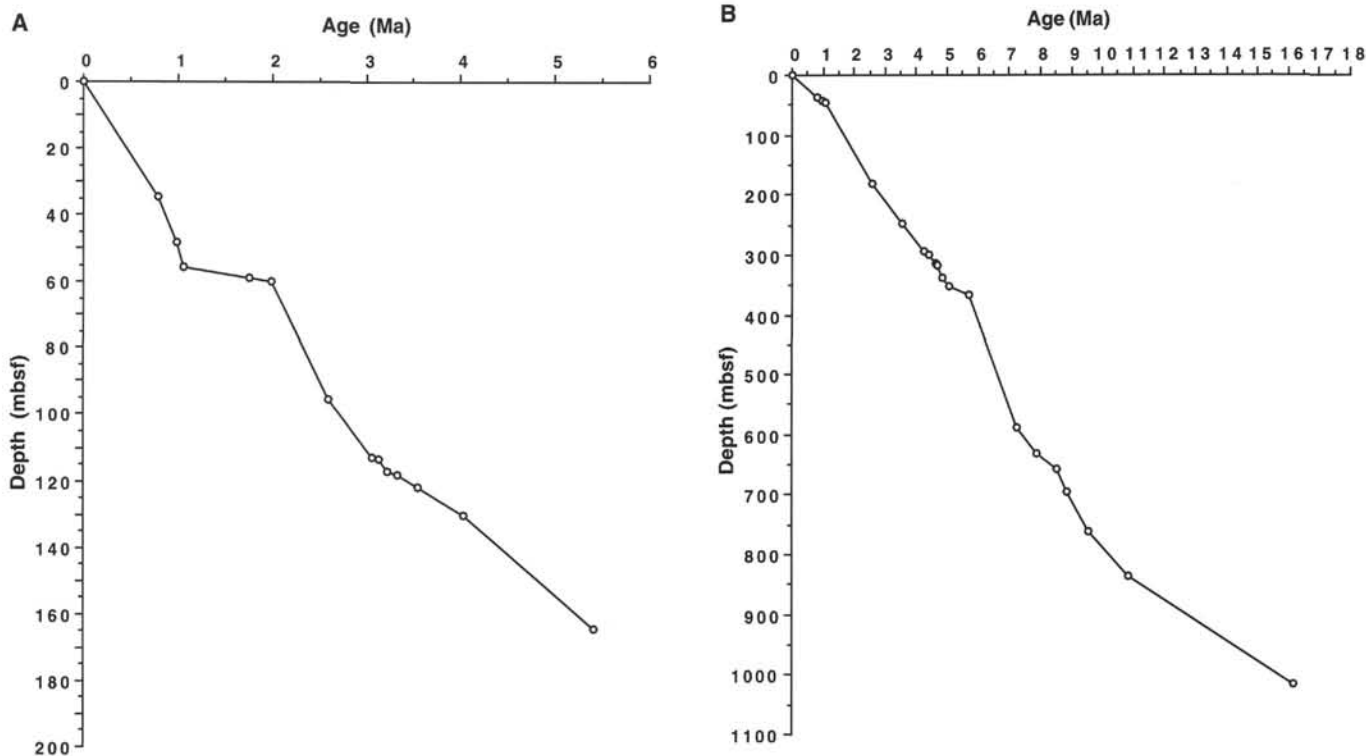


Figure 6. Sedimentation rates for (A) Site 908 and (B) Site 909.

Table 3. Site 908: bulk accumulation rate, linear sedimentation rate, %CaCO<sub>3</sub>, %TOC, and %sand.

Core, section, interval (cm)	Depth (mbsf)	Age (Ma)	Linear sed. rate (cm/m.y.)	Dry bulk density (g/cm <sup>3</sup> )	Bulk accum. rate (g/cm <sup>2</sup> /m.y.)	CaCO <sub>3</sub> accum. rate (g/cm <sup>2</sup> /m.y.)	TOC accum. rate (g/cm <sup>2</sup> /m.y.)	>63- $\mu$ m accum. rate (g/cm <sup>2</sup> /m.y.)	CaCO <sub>3</sub> (wt%)	TOC (wt%)	>63 $\mu$ m (wt%)
1H-1, 10-12	0.11	0.002	4417	1.30	5755.09	84.884	27.39	667.00	1.47	0.48	11.59
1H-1, 33-35	0.33	0.008	4417	1.30	5742.10	505.30	510.34		8.80	0.18	
1H-1, 48-51	0.50	0.011	4417	1.03	4549.51	207.458		2465.38	4.56		54.19
1H-1, 90-93	0.92	0.021	4417	1.31	5800.95	85.561	11.20	910.94	1.47	0.19	15.70
1H-1, 140-143	1.42	0.032	4417	1.31	5786.27	4.050		2082.48	0.07		35.99
1H-2, 10-12	1.61	0.037	4417	1.32	5838.56	51.572	26.27	1714.63	0.88	0.45	29.37
1H-2, 36-37	1.86	0.043	4417	1.32	5830.44	116.609	78.71		2.00	1.35	
1H-2, 48-51	1.98	0.046	4417	1.32	5830.44	465.135			7.98		
1H-2, 92-94	2.43	0.056	4417	1.09	4814.53	44.131	13.29	279.75	0.92	0.28	5.81
1H-2, 142-144	2.93	0.067	4417	1.09	4814.53	28.406		344.24	0.59		7.15
1H-3, 9-11	3.10	0.071	4417	1.34	5915.39	43.378	28.33	2515.38	0.73	0.48	42.52
1H-3, 49-51	3.50	0.080	4417	1.34	5918.78	11.838		1691.59	0.20		28.58
1H-3, 91-93	3.92	0.090	4417	1.41	6227.97	52.936	10.65	2068.62	0.85	0.17	33.21
1H-3, 108-140	4.08	0.094	4417	1.41	6227.97	12.456	18.06		0.20	0.29	
1H-4, 138-140	4.39	0.101	4417	1.41	6227.97	15.570		3187.48	0.25		51.18
1H-4, 9-11	4.60	0.106	4417	1.36	5986.94	51.885	50.23	916.21	0.87	0.84	15.30
1H-4, 35-37	4.85	0.112	4417	1.36	6007.12	132.157	17.42		2.20	0.29	
1H-5, 52-54	5.03	0.116	4417	1.36	6007.12	34.841		1577.47	0.58		26.26
1H-CC, 8-10	5.26	0.121	4417	1.36	6016.66	14.540	12.88	891.36	0.24	0.21	14.81
2H-1, 10-11	5.51	0.127	4417	1.36	6027.65	26.621	22.78	1997.16	0.44	0.38	33.13
2H-1, 18-20	5.58	0.129	4417	1.36	6007.12	12.014	19.22		0.20	0.32	
2H-1, 91-93	6.32	0.145	4417	1.49	6581.33	124.492	62.06	2062.39	1.89	0.94	31.34
2H-1, 96-98	6.36	0.146	4417	1.49	6581.33	144.789	103.99		2.20	1.58	
2H-1, 140-144	6.82	0.157	4417	1.49	6581.33	98.720		2419.96	1.50		36.77
2H-2, 9-11	7.00	0.161	4417	1.52	6713.84	95.109	23.23	1127.76	1.42	0.35	16.80
2H-2, 40-42	7.30	0.168	4417	1.52	6713.84	80.566	49.01		1.20	0.73	
2H-2, 49-51	7.40	0.170	4417	1.52	6713.84	117.492		3036.67	1.75		45.23
2H-2, 82-94	7.83	0.180	4417	1.54	6802.18	9.069	22.11	569.84	0.13	0.33	8.38
2H-2, 141-142	8.32	0.191	4417	1.54	6802.18	21.087	0.00	1104.67	0.31		16.24
2H-3, 11-13	8.52	0.196	4417	1.22	5388.74	112.710	15.47	1367.75	2.09	0.29	25.38
2H-3, 24-26	8.64	0.199	4417	1.22	5388.74	37.721	21.02		0.70	0.39	
2H-3, 47-49	8.87	0.204	4417	1.22	5388.74	15.613			0.29		
2H-3, 140-142	9.81	0.226	4417	1.22	5388.74	212.855		2050.95	3.95		38.06
2H-4, 9-12	10.01	0.230	4417	1.50	6625.50	97.170	20.47	1454.26	1.47	0.31	21.95
2H-4, 44-46	10.34	0.238	4417	1.50	6625.50	72.881	25.18		1.10	0.38	
2H-4, 49-52	10.39	0.239	4417	1.50	6625.50	83.537			1.26		
2H-4, 90-93	10.82	0.249	4417	1.18	5212.06	29.534	19.18	2691.22	0.57	0.37	51.63
2H-4, 142-145	11.33	0.261	4417	1.18	5212.06	25.539		1352.53	0.49		25.95
2H-5, 8-11	11.50	0.265	4417	1.52	6713.84	205.883	44.45	2237.98	3.07	0.66	33.33
2H-5, 38-40	11.78	0.271	4417	1.52	6713.84	46.997	45.65		0.70	0.68	
2H-5, 44-47	11.86	0.273	4417	1.52	6713.84	47.668		1908.74	0.71		28.43
2H-5, 90-93	12.32	0.284	4417	1.52	6713.84	115.809	46.46	1383.29	1.72	0.69	20.60
2H-5, 138-141	12.78	0.294	4417	1.52	6713.84	59.039			0.88		
2H-6, 138-141	12.80	0.295	4417	1.52	6713.84	46.325		1981.93	0.69		29.52
2H-6, 8-11	13.00	0.299	4417	1.48	6537.16	3.268	44.06	2238.17	0.05	0.67	34.24
2H-6, 35-37	13.25	0.305	4417	1.48	6537.16	91.520	56.87		1.40	0.87	
2H-6, 48-51	13.40	0.308	4417	1.48	6537.16	105.902		2254.01	1.62		34.48
2H-6, 92-95	13.84	0.319	4417	1.48	6537.16	49.027	26.48	371.64	0.75	0.41	5.69
2H-7, 138-141	14.30	0.329	4417	1.48	6537.16	20.265			0.31		
2H-7, 24-26	14.65	0.337	4417	1.48	6537.16	20.919			0.32		
2H-7, 40-42	14.80	0.341	4417	1.48	6537.16	58.834	21.57		0.90	0.33	
2H-7, 59-61	15.00	0.345	4417	1.46	6448.82	54.813	12.12	3701.16	0.85	0.19	57.39
2H-1, 9-11	15.00	0.345	4417	1.46	6448.82	35.467	12.90	3701.16	0.55	0.20	57.39
2H-CC, 9-12	15.24	0.351	4417	1.46	6448.82	70.397	15.15	2466.68	1.09	0.24	38.25
3H-1, 54-56	15.44	0.356	4417	1.46	6448.82	4.463			0.07		
3H-1, 82-84	15.72	0.362	4417	1.46	6448.82	51.591	29.66		0.80	0.46	
3H-1, 90-93	15.82	0.365	4417	1.44	6367.30	65.793	30.05	1353.87	1.03	0.47	21.26
3H-1, 140-143	16.32	0.376	4417	1.44	6360.48	5.088		456.05	0.08		7.17
3H-2, 9-11	16.50	0.380	4417	1.70	7508.90	72.583	38.00	849.76	0.97	0.51	11.32
3H-2, 49-52	16.89	0.389	4417	1.70	7508.90	69.681			0.93		
3H-2, 75-77	17.15	0.395	4417	1.70	7508.90	45.053	46.56		0.60	0.62	
3H-2, 93-96	17.35	0.400	4417	1.45	6401.68	81.618	44.43	2117.15	1.27	0.69	33.07
3H-2, 140-143	17.82	0.410	4417	1.45	6404.65	22.416		2212.17	0.35		34.54
3H-3, 9-11	18.00	0.415	4417	1.45	6415.24	20.849	21.17	827.69	0.32	0.33	12.90
3H-3, 29-31	18.19	0.419	4417	1.05	4615.77	13.847	14.77		0.30	0.32	
3H-3, 49-52	18.39	0.424	4417	1.05	4615.77	3.383			0.07		
3H-3, 90-93	18.82	0.434	4417	1.46	6431.50	65.920	12.54	3374.56	1.02	0.20	52.47
3H-3, 145-148	19.35	0.446	4417	1.46	6431.50	46.619			0.72		
3H-4, 9-11	19.50	0.449	4417	1.46	6431.50	34.300	27.46	1923.70	0.53	0.43	29.91
3H-4, 38-40	19.78	0.456	4417	1.46	6431.50	19.295	41.16		0.30	0.64	
3H-4, 47-50	19.87	0.458	4417	1.46	6431.50	46.090			0.72		
3H-4, 47-50	19.89	0.458	4417	1.46	6448.82	23.216		562.34	0.36		8.72
3H-4, 93-96	20.35	0.469	4417	1.46	6459.42	25.837	34.88	665.99	0.40	0.54	10.31
3H-4, 140-143	20.82	0.480	4417	1.46	6448.82	18.702		873.82	0.29		13.55
3H-5, 9-11	21.00	0.484	4417	1.46	6470.37	93.277	46.13	1058.30	1.44	0.71	16.36
3H-5, 33-35	21.23	0.489	4417	1.46	6448.82	90.283	41.92		1.40	0.65	
3H-5, 46-49	21.38	0.493	4417	1.46	6448.82	30.954			0.48		
3H-5, 93-96	21.85	0.503	4417	1.47	6483.91	66.998	28.79	1378.54	1.03	0.44	21.26
3H-5, 140-143	22.32	0.514	4417	1.47	6492.99	20.128		696.05	0.31		10.72
3H-6, 9-11	22.50	0.518	4417	1.47	6493.68	59.523	32.40	821.51	0.92	0.50	12.65

Notes: sed. = sedimentation, accum. = accumulation.

Only part of this table is produced here. The entire table appears on the CD-ROM.

Table 4. Site 909: bulk accumulation rate, linear sedimentation rate, %CaCO<sub>3</sub>, %TOC, and %sand.

Core, section, interval (cm)	Depth (mbsf)	Age (Ma)	Linear sed. rate (cm/m.y.)	Dry bulk density (g/cm <sup>3</sup> )	Bulk accum. rate (g/cm <sup>2</sup> /m.y.)	CaCO <sub>3</sub> accum. rate (g/cm <sup>2</sup> /m.y.)	TOC accum. rate (g/cm <sup>2</sup> /m.y.)	>63- $\mu$ m accum. rate (gm/cm <sup>2</sup> /m.y.)	CaCO <sub>3</sub> (wt%)	TOC (wt%)	> 63 $\mu$ m (wt%)
	47.10	1.050	8681								
1R-1, 14-16	85.15	1.488	8681	1.35	11720.02	34.61			0.30		
1R-1, 29-30	85.30	1.490	8681	1.35	11720.02	82.04	84.38		0.70	0.72	
1R-1, 64-66	85.65	1.494	8681	1.33	11546.39	76.01	90.99	1248.05	0.66	0.79	10.81
3R-1, 33-34	104.64	1.713	8681	1.4	12154.09	24.31	54.69		0.20	0.45	
3R-1, 64-66	104.95	1.716	8681	1.56	13543.13	0.001	48.97	632.28	0.00	1.10	4.67
3R-2, 33-34	106.14	1.730	8681	1.45	12588.17	100.71	110.78		0.80	0.88	
3R-2, 64-66	106.45	1.734	8681	1.33	11546.39	62.54	84.29	1019.64	0.54	0.73	8.83
4R-1, 27-28	114.18	1.823	8681	1.32	11459.57	263.57	143.24		2.30	1.25	
4R-1, 64-66	114.55	1.827	8681	1.32	11459.57	408.71	40.22	490.58	3.57	0.35	4.28
4R-2, 64-66	116.05	1.844	8681	1.44	12501.35	135.43	95.51	1129.47	1.08	0.76	9.03
4R-3, 27-28	117.11	1.856	8681	1.42	12327.72	147.93	122.04		1.20	0.99	
5R-1, 19-21	123.80	1.933	8681	1.41	12240.91	7.14	47.62	2469.51	0.06	0.39	20.17
5R-1, 32-33	123.93	1.935	8681	1.41	12240.91	48.96	101.60		0.40	0.83	
6R-1, 38-39	133.59	2.046	8681	1.42	12327.72	24.66	53.01		0.20	0.43	
6R-1, 64-66	133.85	2.049	8681	1.42	12327.72	102.73	86.17	1211.44	0.83	0.70	9.83
6R-2, 64-66	135.35	2.067	8681	1.38	11980.46	71.88	86.50	1336.97	0.60	0.72	11.16
6R-3, 38-39	136.59	2.081	8681	1.4	12154.09	449.70	29.17		3.70	0.24	
6R-3, 64-66	136.85	2.084	8681	1.43	12414.54	80.69	112.97	1189.02	0.65	0.91	9.58
7R-1, 32-33	143.23	2.157	8681	1.43	12414.54	62.07	100.56		0.50	0.81	
7R-1, 48-49	143.39	2.159	8681	1.44	12501.35	3637.89	116.26		29.10	0.93	
7R-1, 65-67	143.56	2.161	8681	1.45	12588.17	69.23	103.73	574.50	0.55	0.82	4.56
7R-2, 65-67	145.06	2.178	8681	1.38	11980.46	118.80	112.74	331.84	0.99	0.94	2.77
7R-3, 14-16	146.05	2.190	8681	1.38	11980.46	73.37			0.61		
7R-3, 23-24	146.14	2.191	8681	1.41	12240.91	159.13	80.79		1.30	0.66	
7R-3, 65-67	146.56	2.196	8681	1.44	12501.35	152.09	87.38	697.08	1.22	0.70	5.58
7R-4, 55-56	147.96	2.212	8681	1.41	12240.91	3231.60	117.51		26.40	0.96	
7R-4, 65-67	148.06	2.213	8681	1.39	12067.28	126.70	82.30	1510.65	1.05	0.68	12.52
8R-1, 39-40	153.00	2.270	8681	1.37	11893.65	23.79	173.65		0.20	1.46	
8R-1, 65-67	153.26	2.273	8681	1.34	11633.20	116.33	143.09	322.53	1.00	1.23	2.77
8R-2, 65-67	154.76	2.290	8681	1.37	11893.65	247.77	130.83	793.66	2.08	1.10	6.67
8R-3, 4-5	155.65	2.300	8681	1.37	11893.65	83.26	114.18		0.70	0.96	
8R-3, 10-11	155.71	2.301	8681	1.37	11893.65	975.28	96.34		8.20	0.81	
8R-3, 14-15	155.75	2.301	8681	1.38	11980.46	1641.32	106.63		13.70	0.89	
8R-3, 18-19	155.79	2.302	8681	1.39	12067.28	120.67	106.19		1.00	0.88	
8R-3, 28-29	155.89	2.303	8681	1.41	12240.91	146.89	110.17		1.20	0.90	
8R-3, 65-67	156.26	2.307	8681	1.44	12501.35	42.71	115.76	735.80	0.34	0.93	5.89
8R-4, 14-16	157.25	2.319	8681	1.44	12501.35	64.31			0.51		
8R-4, 65-67	157.76	2.325	8681	1.39	12067.28	69.38	98.83	596.78	0.57	0.82	4.95
8R-5, 65-67	159.26	2.342	8681	1.47	12761.80	96.77	122.39	148.93	0.76	0.96	1.17
8R-5, 82-83	159.43	2.344	8681	1.3	11285.94	67.72	84.64		0.60	0.75	
9R-1, 28-29	162.59	2.380	8681	1.32	11459.57	171.89	136.37		1.50	1.19	
9R-1, 64-66	162.95	2.384	8681	1.28	11112.31	206.50	100.79	755.33	1.86	0.91	6.80
9R-1, 91-92	163.22	2.387	8681	1.29	11199.13	2766.19	70.55		24.70	0.63	
9R-1, 96-97	163.27	2.388	8681	1.31	11372.76	193.34	159.22		1.70	1.40	
9R-2, 29-30	164.10	2.398	8681	1.34	11633.20	139.60	108.19		1.20	0.93	
9R-2, 64-66	164.45	2.402	8681	1.37	11893.65	148.66	145.10	292.05	1.25	1.22	2.46
9R-3, 28-29	165.59	2.415	8681	1.29	11199.13	78.39	97.43		0.70	0.87	
9R-3, 64-66	165.95	2.419	8681	1.2	10417.79	329.88	125.01	410.36	3.17	1.20	3.94
9R-3, 134-135	166.65	2.427	8681	1.28	11112.31	3122.56	91.12		28.10	0.82	
9R-3, 142-143	166.73	2.428	8681	1.35	11720.02	234.40	147.67		2.00	1.26	
9R-4, 28-29	167.09	2.432	8681	1.4	12154.09	72.92	55.91		0.60	0.46	
9R-4, 64-66	167.45	2.436	8681	1.43	12414.54	92.07	105.03	1198.93	0.74	0.85	9.66
10R-1, 23-24	172.14	2.490	8681	1.5	13022.24	403.69	135.43		3.10	1.04	
10R-1, 64-66	172.55	2.495	8681	1.73	15018.99	127.66	114.59	608.11	0.85	0.76	4.05
10R-2, 64-66	174.05	2.512	8681	1.46	12674.98	351.72	102.29	4217.21	2.77	0.81	33.27
10R-3, 31-32	175.22	2.526	8681	1.46	12674.98	722.47	168.58		5.70	1.33	
10R-3, 64-66	175.55	2.530	8681	1.46	12674.98	70.77	68.57	7083.94	0.56	0.54	55.89
10R-4, 54-56	176.95	2.546	8681	1.51	13109.06	132.18	86.13	518.41	1.01	0.66	3.95
10R-4, 64-66	177.05	2.547	8681	1.47	12761.80	55.30	79.12	491.56	0.43	0.62	3.85
10R-5, 28-29	178.19	2.560	8681	1.44	12501.35	237.53	133.76		1.90	1.07	
10R-5, 64-66	178.55	2.564	8681	1.42	12327.72	173.61	98.50	752.37	1.41	0.80	6.10
10R-6, 0-1	179.41	2.574	8681	1.41	2154.09	85.08	119.11		0.70	0.98	
10R-6, 64-66	180.05	2.581	8681	1.38	11980.46	45.92	89.01	823.09	0.38	0.74	6.87
10R-7, 39-40	181.30	2.596	8681	1.38	11980.46	203.67	129.39		1.70	1.08	
11R-1, 14-15	181.75	2.601	8681	1.39	12067.28	168.94	108.61		1.40	0.90	
	181.75	2.601	6847	1.39	9517.05						
11R-1, 65-67	182.26	2.608	6847	1.39	9517.05	149.09	91.55	351.29	1.57	0.96	3.69
11R-2, 64-66	183.75	2.630	6847	1.37	9380.12	79.73	83.20	625.93	0.85	0.89	6.67
11R-3, 64-66	185.25	2.652	6847	1.39	9517.05	2178.52	50.73	6.77	22.89	0.53	0.07
11R-3, 80-81	185.41	2.654	6847	1.41	9653.99	96.54	101.37		1.00	1.05	
11R-4, 64-66	186.75	2.674	6847	1.43	9790.92	120.75	89.29	599.64	1.23	0.91	6.12
11R-5, 64-66	188.25	2.696	6847	1.73	11844.96	0.00	81.37	3458.53	0.00	0.69	29.20
11R-5, 81-82	188.42	2.698	6847	1.52	10407.14	176.92	100.95		1.70	0.97	
11R-6, 64-66	189.75	2.718	6847	1.51	10338.67	96.49	76.92	1222.97	0.93	0.74	11.83
12R-1, 64-66	191.85	2.749	6847	1.64	11228.75	121.64	128.01	897.19	1.08	1.14	7.99
12R-1, 86-87	192.07	2.752	6847	1.52	10407.14	634.84	149.86		6.10	1.44	
12R-2, 64-66	193.35	2.770	6847	1.47	10064.80	15.10	81.93	427.74	0.15	0.81	4.25
12R-3, 64-66	194.85	2.792	6847	1.37	9380.12	78.16	97.55	369.57	0.83	1.04	3.94
12R-3, 91-92	195.12	2.796	6847	1.37	9380.12	93.80	93.80		1.00	1.00	
12R-4, 64-55	196.35	2.814	6847	1.37	9380.12	46.90	97.55	660.93	0.50	1.04	7.05
12R-5, 30-31	197.51	2.831	6847	1.41	9653.99	67.58	109.09		0.70	1.13	
12R-5, 64-66	197.85	2.836	6847	1.42	9722.46	0.00	94.31	658.77	0.00	0.97	6.78

Notes: sed. = sedimentation, accum. = accumulation.

Only part of this table is produced here. The entire table appears on the CD-ROM.

the carbonate percent, and are further supported by the changes in sand composition (see Wolf-Welling et al., this volume).

In addition to the sedimentological changes observed here, there is evidence gathered elsewhere in the North Atlantic for ice sheet build-up during this time. Schaeffer and Spiegler (1986) report ice-rafting events at 10.2 and 8.0 m.y. at Site 408, and Wolf and Thiede (1991) document ice rafting starting at 9.5 m.y. at Site 646. Stage II also spans the time of the first dropstones recovered on the East Greenland Margin (7 m.y.; Larsen, Saunders, Clift, et al., 1994) and just before the oldest dropstone recovered off of Iceland (6 m.y.; Myhre, Thiede, Firth, et al., 1995).

Unfortunately, there is some ambiguity in the interpretation of these results. The primary signal should be variations in sediment supply through weathering changes on land and through ice rafting. Increased ice rafting should produce an increase in the coarse fraction and indicate glacial conditions, and the coarse fraction is usually considered to be a proxy for ice rafting.

In other areas (e.g., Kaneps, 1979), however, increased coarse fraction is attributed to increasing current velocity as finer sediments are winnowed away. Here, that could indicate the strength of deep-water flow through Fram Strait. However, the coarse fraction may also be due to increases in ice-rafted sediment. It is difficult to distinguish bottom current activity and ice rafting in this area.

In other areas, increases in bulk accumulation are considered to be indicative of glacial transport, especially when accompanied by high sand accumulation (e.g., Henrich et al., 1989). Separating the current velocity signal from the ice-rafting signal is not easily done, although McCave et al. (1995), have shown that it is possible with painstaking composition and size analyses of different size fractions. Another possibility for distinguishing bottom current flow from ice-rafted sediment is to compare the same age sediments from shallow- and deep-water sites, and assume that if both size and composition are the same, then ice/glaciation dominates. If they differ, it is likely to be caused by the increased importance of bottom currents.

In the upper part of Stage II (6.2–5.7 m.y.), sediments were recovered from both sites. The interval of 6.2–6.0 m.y. (Site 909) shows a high accumulation rate, with relatively low sand and carbonate accumulation rates. In contrast, although the bulk accumulation rate is low at Site 908, the coarse fraction and carbonate accumulation rates and wt% are relatively high. Unfortunately, without more of the older record, it is difficult to discern which is ice rafting and which is current. There may be intermediate depth currents (Site 908) reworking the glacially influenced deposition.

It is also interesting to speculate about other climatic and oceanographic events beyond the Arctic region during the late part of stage II. For example, it is estimated that the first drawdown of the Mediterranean took place between 7.1 and 7.3 m.y. (El-Hawat, 1995), suggesting a lowered sea level and increased mid-latitude aridity, an aridity that might in part be caused by Arctic glaciation. On the Haq et al. (1987) cycle chart, one of the six major Cenozoic second-order supercycle boundaries occurred within this time interval near the middle/late Miocene boundary. The sea level lowering at the supercycle boundary supports ice build-up during this time.

Stage III ranges from upper Miocene to middle Pliocene (Site 909: 368–200 mbsf, Site 908, 167–105 mbsf; 5.7–2.8 m.y.) and represents the first opportunity to examine sedimentological differences with depth. Dropstones first occur in this interval. At Site 909, an isolated dropstone occurs at 314 mbsf (4.6 m.y.), and they become common above 233 mbsf (3.4 m.y.). At Site 908, dropstones begin at 139 mbsf (4.5 m.y.). Accumulation rates are highly variable at Site 909 and are relatively constant at Site 908. Coarse fraction accumulation rates are low at both sites. However, coarse fraction percentage is always below 20% at Site 909; whereas, at the shallower site (Site 908), coarse fraction percentage fluctuates between a few percent and 60%, and >40% occurs near 6.25, 4.25, and 3.55 m.y. In addition, at Site 908 before and after 4.2 m.y. there is a minor change in lithology that is not seen at Site 909. At Site 908, between 4.2 and 2.8 m.y., there is

a slight increase in sand accumulation, and the overall low carbonate values are slightly higher.

The time represented by this interval is also one of major paleoclimatic and paleoceanographic change. The isthmus of Panama closed in the early to middle Pliocene (Wolf and Thiede, 1991), and at 4.2 m.y. there is an isotopic divergence between planktonic foraminifers in the Caribbean and Panamanian basins (Raymo et al., 1992). This interval at Fram Strait, with its reduced bulk and coarse accumulation rates, may suggest a decrease in glaciation associated with the warming trend.

Stage IV represents the middle Pliocene to the present (<2.8 m.y., Site 909: 200–0 mbsf; Site 908: 105–0 mbsf). It contains high-amplitude variations in coarse fraction and %TOC but overall moderate bulk accumulation rates. These variations are attributable to the glacial-interglacial fluctuations occurring at this time. Some of the chemical data suggests that there are differences in the source areas for the two sites. At Site 909 there is a change in the wt% of K<sub>2</sub>O in the sediment from average values of 2.7–2.8 below about 220 mbsf (3.17 m.y.) to average values of 3.3 to 3.4 above 180 mbsf (2.6 m.y.). At Site 908, there is a steady increase in the wt% of K<sub>2</sub>O beginning at 175 mbsf (5.8 m.y.; Myhre, Thiede, Firth, et al., 1995).

Bulk accumulation rates are higher at Site 909 in the early part of Stage I, between 2.8 and 1.0 m.y., an interval that includes very low accumulation rates (570–800 gcm<sup>-2</sup>m.y.<sup>-1</sup> between 2.0 and 1.1 m.y.) at Site 908. There are no sedimentary clues to help to determine whether the decrease in bulk accumulation rate at Site 908 is caused by erosion or nondeposition. For example, at Site 909 there is no indication of slumped sediment or of a change in accumulation rate, to suggest mass wasting of Site 908 sediment to Site 909.

During the uppermost 1 m.y., both sites show an overall decrease in bulk accumulation, with roughly equivalent rates. However, the coarse fraction accumulation rates are higher and more variable at Site 908 than at Site 909. At Site 909, there is also an overall decrease in the variability of CaCO<sub>3</sub> accumulation, attributed to the lack of carbonate-rich layers. This is especially true for the last 1 m.y. At Site 908, CaCO<sub>3</sub> accumulation rates are an order of magnitude lower, and, except for two CaCO<sub>3</sub>-rich layers at the very top, also show little variation in CaCO<sub>3</sub> accumulation rates.

In summary, the four stages discussed here represent major paleoceanographic and paleoclimatic changes in the Northern Hemisphere. Each of these intervals needs to be studied in more detail at both higher temporal and spatial resolutions.

## ACKNOWLEDGMENTS

The assistance of the captain, crew, and technical staff of the *JOIDES Resolution* on Leg 151 in obtaining samples is gratefully acknowledged. Paul Albert, Claire Hruby, Robin Park, and Elena Proakis assisted with various portions of the laboratory analyses. Joel LaBella kept the coulometer running. Gerhard Bohrmann and an anonymous reviewer provided comments that substantially improved this paper. This work was funded by a grant from the J.O.I. - U.S. Science Advisory Committee to Suzanne O'Connell.

## REFERENCES

- Davies, T.A., Hay, W.W., Southam, J.R., Worsley, T.R., 1977. Estimates of Cenozoic oceanic sedimentation rates. *Science*, 197:53–55.
- El-Hawat, A.S., 1995. Report on conference on the Messinian Event. *IAS Newsl.*, 138:8.
- Haq, B.U., Hardenbol, J., and Vail, P.R., 1987. Chronology of fluctuating sea levels since the Triassic. *Science*, 235:1156–1167.
- Henrich, R., Wolf, T., Bohrmann, G., and Thiede, J., 1989. Cenozoic paleoclimatic and paleoceanographic changes in the Northern Hemisphere revealed by variability of coarse-fraction composition in sediments from the Vøring Plateau ODP Leg 104 drill sites. In Eldholm, O., Thiede, J., Taylor, E., et al., *Proc. ODP, Sci. Results*, 104: College Station, TX (Ocean Drilling Program), 75–188.

Huffman, E.W.D., 1977. Performance of a new automatic carbon dioxide coulometer. *Microchem. J.*, 22:567-573.

Kaneps, A.G., 1979. Gulf Stream: velocity fluctuations during the late Cenozoic. *Science*, 204:297-301.

Kristoffersen, Y., 1990. On the tectonic evolution and paleoceanographic significance of the Fram Strait gateway. In Bleil, U., and Thiede, J. (Eds.), *Geological History of the Polar Oceans: Arctic versus Antarctic*. NATO ASI Ser., Ser. C, 308:63-76.

Larsen, H.C., Saunders, A.D., Clift, P.D., et al., 1994. *Proc. ODP, Init. Repts.*, 152: College Station, TX (Ocean Drilling Program).

McCave, I.N., Manighetti, B., and Robinson, S., 1995. Sortable silt and fine sediment size/composition slicing: parameters for palaeocean speed and palaeoceanography. *Paleoceanography*, 10:593-609.

Myhre, A.M., Thiede, J., Firth, J.V., et al., 1995. *Proc. ODP, Init. Repts.*, 151: College Station, TX (Ocean Drilling Program).

Raymo, M.E., Hodell, D., and Jansen, E., 1992. Response of deep ocean circulation to initiation of Northern Hemisphere glaciation (3-2 Ma). *Paleoceanography*, 7:645-672.

Schaeffer, R., and Spiegler, D., 1986. Neogene Kälteeinbrüche und Vereisungsphasen im Nordatlantik. *Z. Dtsch. Geol. Ges.*, 137:537-552.

Swift, J.H., Takahashi, T., and Livingston, H.D., 1983. The contribution of the Greenland and Barents Seas to the deep water of the Arctic Ocean. *J. Geophys. Res.*, 88:5981-5986.

Wolf, T.C.W., and Thiede, J., 1991. History of terrigenous sedimentation during the past 10 m.y. in the North Atlantic (ODP Legs 104 and 105 and DSDP Leg 81). *Mar. Geol.*, 101:83-102.

Date of initial receipt: 6 July 1995  
 Date of acceptance: 18 December 1995  
 Ms 151SR-140

LEG 151 HOLE 908 A

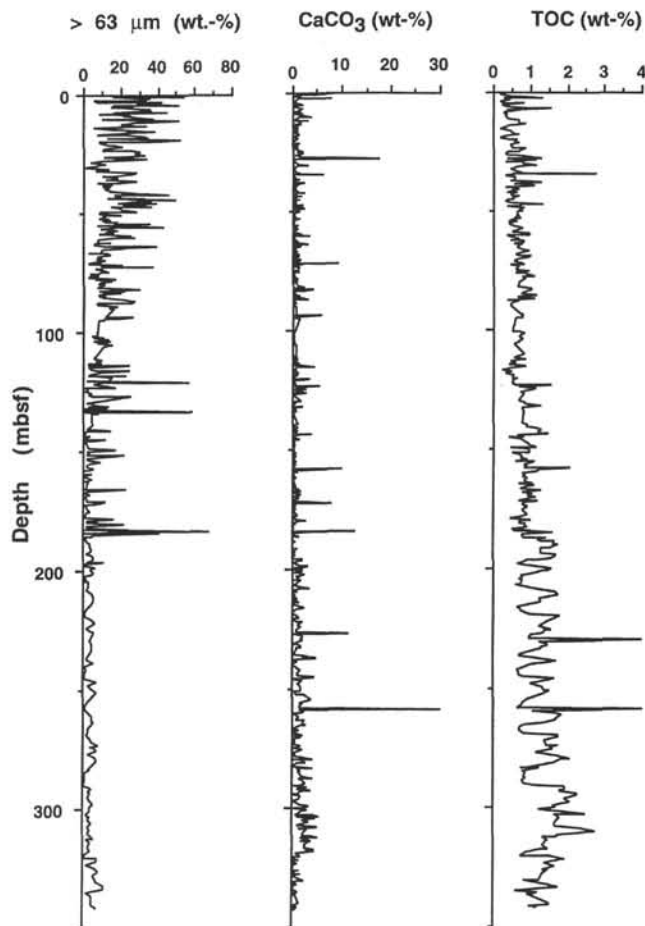


Figure 7. Sediment components plotted vs. depth for Site 908.

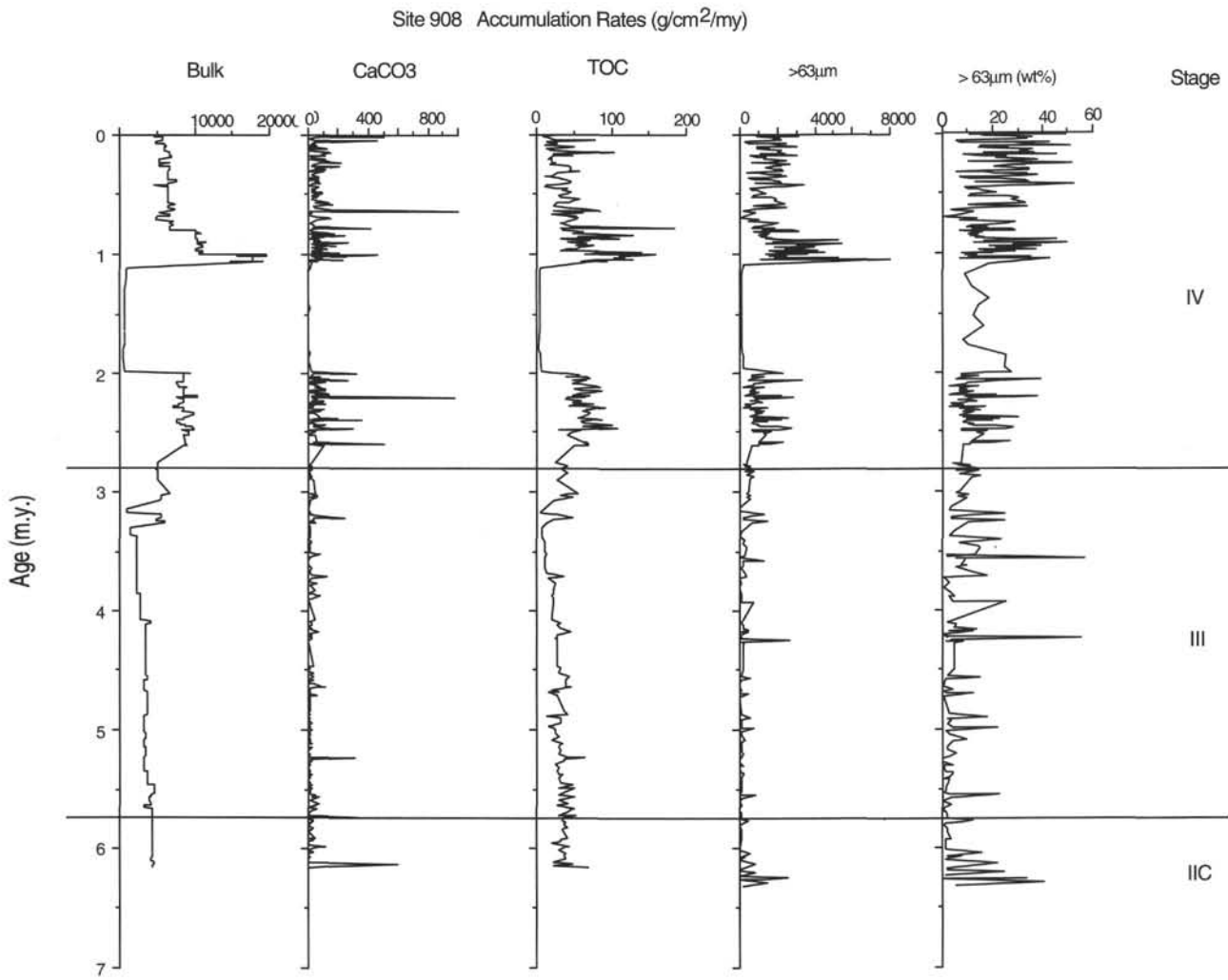


Figure 8. Sediment components plotted vs. age for Site 908.

LEG 151 HOLES 909 A/C

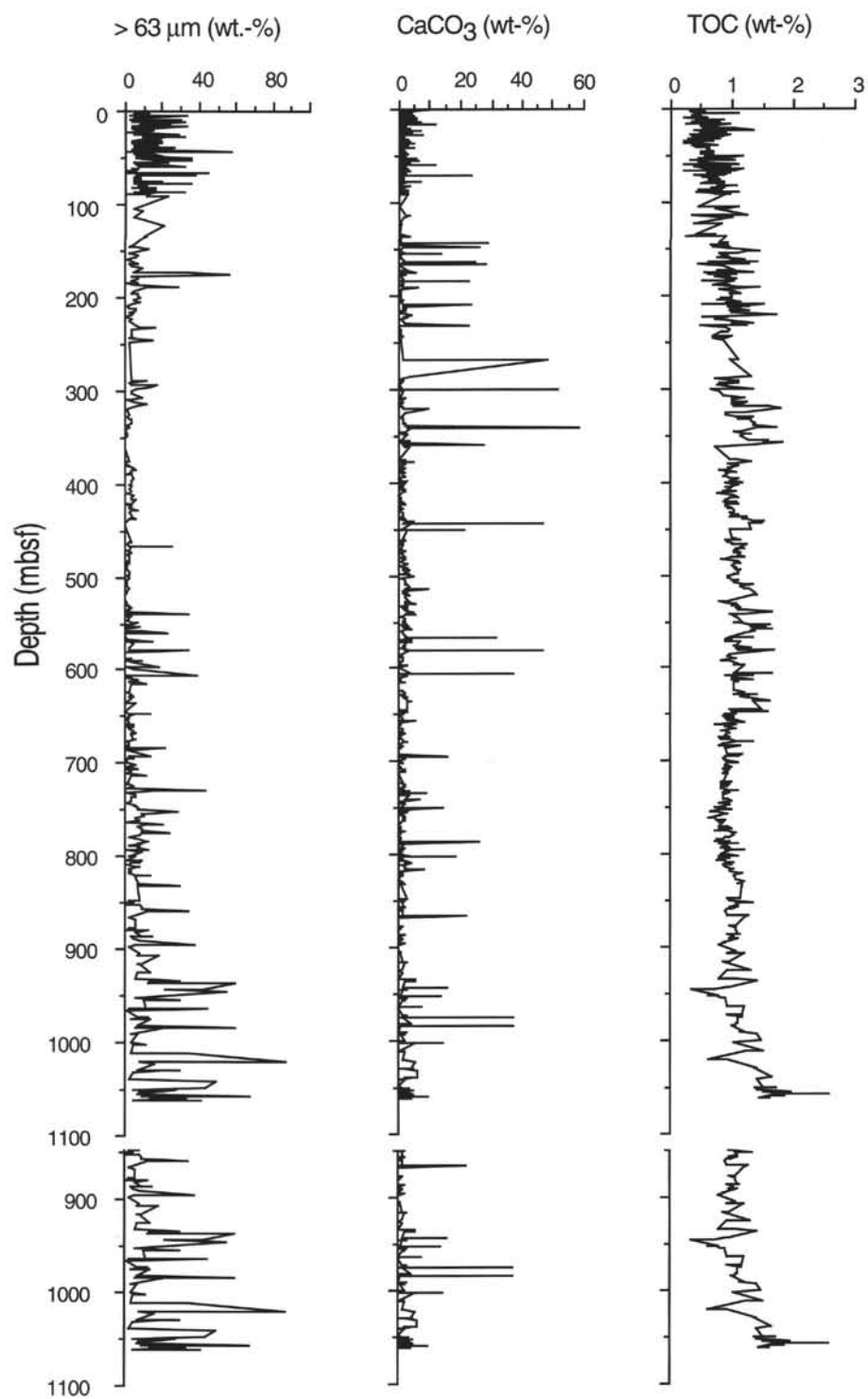


Figure 9. Sediment components plotted vs. depth for Site 909.

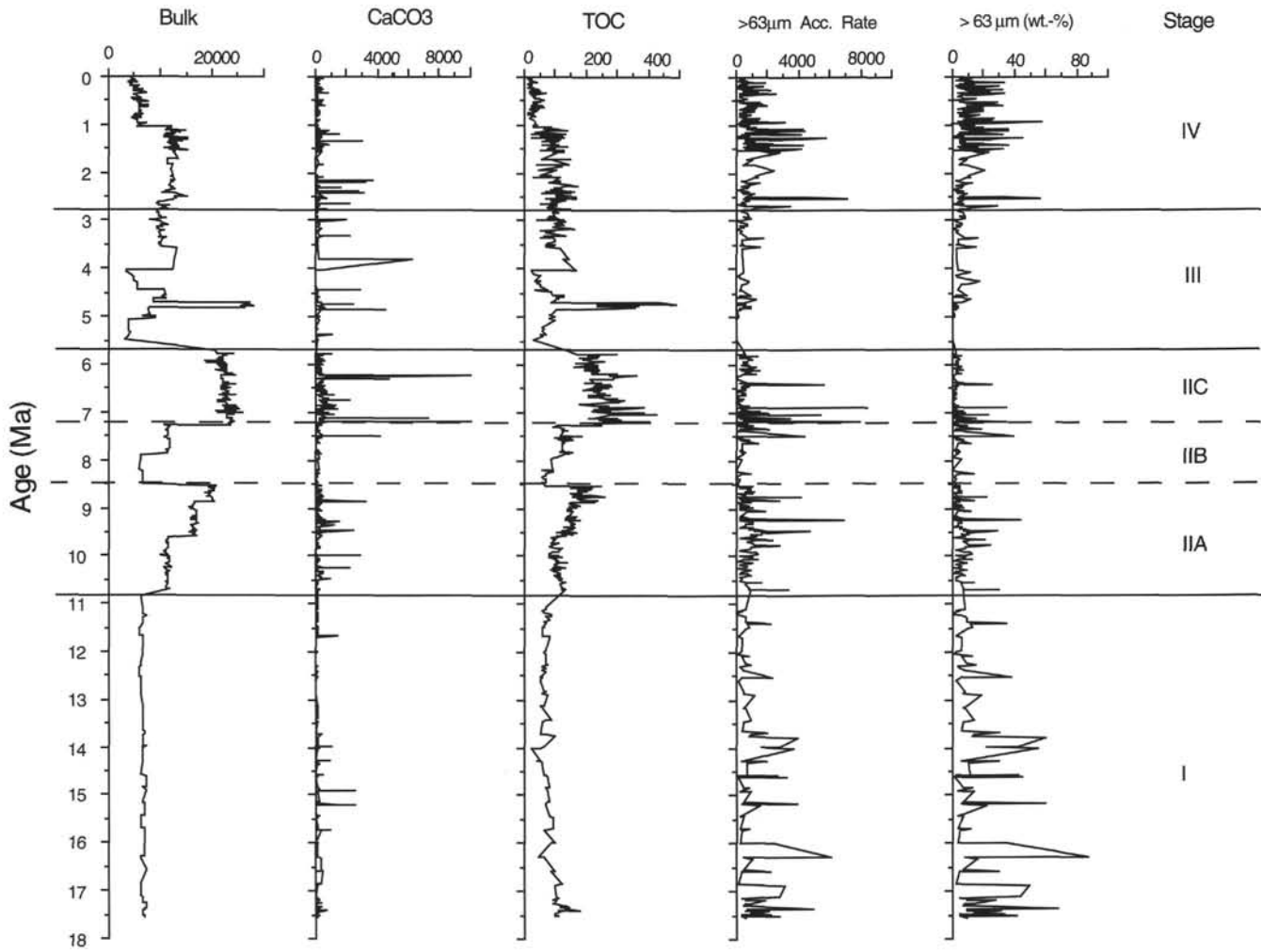
Site 909 Accumulation Rates (g/cm<sup>2</sup>/my)

Figure 10. Sediment components plotted vs. age for Site 909.

**Table 5. Summary of important accumulation rate characteristics of sedimentary stages at Fram Strait.**

	Stage IV	Stage III	Stage II	Stage I	Stage IV	Stage III
	Site 909	Site 909	Site 909	Site 909	Site 908	Site 908
<b>Bulk accumulation rates*</b>						
Min.	9380.12	3517.33	5990.58	5881.57	574.60	911.05
Max.	15018.99	27932.20	25803.90	7285.12	19427.44	6628.30
Mean	11699.33	11096.75	17779.40	6628.30	8440.57	3641.35
Median	11980.46	9893.63	19915.66	6650.18	8181.03	3477.78
St. dev.	1096.16	6895.58	5434.34	311.95	3646.94	1076.97
<b>CaCO<sub>3</sub> accumulation rates*</b>						
Min.	0.00	0.00	0.00	0.00	0.00	0.00
Max.	3637.89	6229.64	11314.79	1394.73	1146.88	237.34
Mean	349.66	355.53	383.59	163.91	71.20	23.74
Median	120.71	123.09	208.60	88.67	43.81	13.48
St. dev.	737.78	843.42	919.49	316.24	110.00	35.69
<b>TOC accumulation rates*</b>						
min.	29.17	25.22	0.00	0.00	0.00	5.72
max.	173.65	487.49	423.18	95.65	182.81	54.29
mean	102.79	124.25	183.03	72.33	53.45	30.09
median	101.16	96.73	184.44	69.37	51.36	30.53
st.dev.	28.70	99.91	76.32	30.94	30.87	11.69
<b>&gt;63-<math>\mu</math>m accumulation rates*</b>						
Min.	6.77	7.09	44.10	46.19	0.00	1.05
Max.	7083.94	1735.16	4664.02	3673.35	5589.27	2091.64
Mean	1071.74	419.44	570.72	595.21	1485.07	260.76
Median	716.44	354.42	479.51	482.18	1252.32	126.33
St. dev.	1269.74	365.59	501.38	567.51	1100.58	332.27

Notes: \* =  $\text{gcm}^{-2}\text{m.y.}^{-1}$